Complex Semantic-Spatial Relation Aided Indoor Target-Directed Exploration

WOO-CHEOL LEE, (Student Member, IEEE), AND HAN-LIM CHOI, (Senior Member, IEEE)

Department of Aerospace Engineering and KI for Robotics, Korea Advanced Institute of Science and Technology, Daejeon 34141, South Korea

Corresponding author: Han-Lim Choi (hanlimc@kaist.ac.kr)

ABSTRACT This paper addresses the problem of target-directed exploration (TDE) in initially unknown and large-scale indoor environments. In such scenarios, the inference on an unknown space can improve the search performance under the assumption that the context of a particular space (i.e., the functional category of the space) is correlated with the existence of a target. The space inference is promising in that there is a strong statistical correlation between the semantic categories of indoor spaces and their adjacency because the spaces are designed to reflect universal human preferences. In this point of view, we propose a novel TDE scheme leveraging the semantic-spatial relations of an indoor floorplan dataset. Whereas existing works dealing with the data-driven space inferences consider only the one-to-one relation statistics of the spaces or utilize heuristic counting-based matching algorithms without building a trainable latent model, we propose the pattern cognitive Multivariate Bernoulli Distribution-based Graphical Space Inference Model (MBD-GSIM). MBD-GSIM efficiently captures the core contexts of the discrete semantic-spatial relations to predict an unknown space by using the latent Multivariate Bernoulli Distribution model. We also suggest utilizing the MBD-GSIM in a cost-utility based frontier exploration scheme for TDE problems. The proposed scheme is constructed in the Robot Operating System (ROS); its efficiency is investigated in the Gazebo simulation environment.

INDEX TERMS Indoor exploration, robot exploration, robotics and automation, indoor environments, inference algorithms, indoor space inference, planning, computation artificial intelligence, semantic-spatial relation.

I. INTRODUCTION

Advances in technologies such as mapping, object recognition, and navigation in the field of robotics open the possibility that autonomous robot systems can be utilized in applications such as service, structural investigation and exploration, and rescue. While such tasks generally require a robot to be able to search a target, in many realistic scenarios, information about the environment and target is often partially given or uncertain.

For exploratory tasks of indoor robots, the cost-utility based frontier exploration strategy has been widely adopted. In the strategy, the key is to design a utility model that varies according to the mission objective. Unlike the cost model, which only requires the pre-observed map information, the utility model is generally hard to obtain because the future

The associate editor coordinating the review of this manuscript and approving it for publication was Yingxiang Liu.

observation (i.e., the target existence in the TDE problem) from the action to be taken must be inferred. Although the conventional cost-utility based robot exploration schemes have generally been developed in the point of speeding up the volumic spatial information gathering, the TDE problem requires to consider qualitative differences of spaces determined by the existence probability of target.

Related to the target existence inference in spaces, the semantic relation of the space and object have been widely used [1]–[7]. [1] and [2]–[4], [7] utilize prior knowledge about the object-spatial relation to designate a most probable location to find the target; however, the region of interest is limited to a pre-observed map. In [5] and [6], the space prediction concept is introduced to cover unknown regions. [5] suggests a heuristic algorithm to match the pre-observed map to the given dataset to provide the most likely category of the unknown space over the frontier of interest. However, because the algorithm is highly dependent on the

prior data, and not on constructing a latent pattern cognitive model, it is limited for understanding the core patterns of a semantic-spatial relation dataset. [6] constructs a probability distribution of space-to-space pair relations, but does not consider the complex relations of more than two spaces. Including the above papers, to the best of the authors' knowledge, existing studies do not suggest a sophisticated pattern-cognitive learning model which can understand the latent patterns of complex semantic-spatial relations from datasets and predict unknown spaces.

With the aforementioned backgrounds, this paper studies: 1) a space inference model, which learns the regularities of complex indoor semantic-spatial relations, to infer the semantic category of space beyond the frontier of interest, and 2) the usage of the inference model for next-goal generation in the way of cost-utility based frontier exploration.

For the space inference, Multivariate Bernoulli Distribution-based Graphical Space Inference Model (MBD-GSIM) is proposed to predict the category of the unknown node beyond the node of interest. MBD-GSIM learns core latent patterns of the indoor navigational graph dataset which is obtained by a domain conversion of the indoor floorplan from 2D Euclidean space to a graph representation with useful node features (i.e., semantic categories of nodes, position of nodes, location of robot, proximity to frontier of nodes). Among the features in the graph representation, the semantic-spatial relation (discrete semantic categories of nodes and their interactions) is exploited by MBD-GSIM. MBD-GSIM efficiently captures the core context of the semantic-spatial relation with two properties: 1) MBD model can effectively parameterize a multivariate Bernoulli graph consisting of Bernoulli (binary) nodes and their high order interactions (i.e., node itself, edges, cliques), and 2) an indoor semantic-spatial relation graph with categorical nodes can be generalized in the form of multivariate Bernoulli graph. Since MBD-GSIM does not rely on the exhaustive graph matching algorithm or one-to-one relation statistics of the spaces, but learns regularities from complex semantic-spatial relation dataset, so higher inference accuracy and faster prediction times are expected. Also, a multi-step prediction is allowed by the rollout technique because MBD-GSIM takes a graph with multiple space nodes as an input.

For the next-goal generation, a method to sophisticatedly integrate the frontier exploration scheme and the MBD-GSIM is introduced. The proposed method inherits exploration transform (ET) based cost map generation scheme ([8], [9]), where the next goal is obtained by following the steepest gradient from the current robot position. Extending the ET, exploration-search transform (EST) generating a cost-utility map that simultaneously reflects the robot travel cost and the concept of the frontier value is suggested. By using MBD-GSIM to estimate the frontier values, the robot can be efficiently guided to the region with high probability of target presence.

In sum, this paper proposes an MBD-GSIM based frontier exploration scheme is proposed for efficient TDE. Our contributions are as follows:

- The suggestion of domain conversion from 2D Euclidean space to a navigational graph in which holds representative information in a concise yet sufficient manner for TDE.
- The suggestion of latent MBD model based space inference method for higher space inference accuracy than conventional methods by efficiently capturing the core context of complex semantic-spatial relations in the navigational graphs.
- The suggestion of EST method that sophisticatedly integrates the concept of the space inference and the cost-utility based exploration strategy.
- The extensive evaluation and comparison with the existing space inference and robot exploration methods in the ROS/Gazebo environment.

The structure of this paper is as follows: Section II is devoted to a comprehensive description of existing works related to our problem. Section III presents the problem statement. In section IV and V, the proposed space inference aided next-goal generation method and MBD-GSIM for space inference method are described, respectively. In section VI, the computational complexity reduction method for the proposed scheme is described. Section VII provides the evaluation. The last section concludes and plans future work.

II. RELATED WORKS
A. TARGET-DIRECTED EXPLORATION
Table 1 shows a comparison between this paper and previous works related to the TDE problem, with the following perspectives:

- Covered scenario
- Inferred unknown information
- Used environmental context information
- Exploration strategy

[10] and [11] first proposed the concept of cost-based frontier exploration for robot exploration, and various frontier exploration strategies such as costmap generation method [8], random tree graph-based method [12], and bio-inspired method [13] for robot exploration considering the path safety are proposed. Even though they do not deal with target search problems, it is worth referring to these works in that the practical exploration schemes are useful for any exploratory tasks including target search problem. [9], [14], [15] combine the object detection method in cost-based exploration methods to obtain target view during exploration. Although they deal with the concept of target search in initially unknown environments, they are not an active target search methods that make inferences about unknown spaces.

Some studies introduced the concept of unseen target localization based on environmental context. [2]–[4] and [18] introduce the methods of inferring the probability in which a target might exist from semantic contextual information in

TABLE 1. Comparison of previous works and this paper. (Abbreviations mean: scen.-scenario, I.U.I.- Inference of unknown information, C.I.U.- Context information usage, O2P-Object to Place relation, P2P-Place to Place relation, use P2P: Whether to use place-to-place relationships, M-P2P: Wheter to use Multiple Place to Place relation, L.P.M-Wheter to use Latent Parameterized Model, E.S.-Exploration Strategy).

		ours	[8], [10]–[13]	[9], [14], [15]	[1], [16]	[7], [17]	[2]–[4], [18]	[19]–[24]	[6], [25]
scen.	exploration	✓	✓	✓	✓	✓	-	✓	✓
	target search	✓	-	✓	✓	✓	✓	-	✓
I.U.I.	place	✓	-	-	-	-	-	✓	✓
	target	✓	-	-	✓	✓	✓	-	✓
C.I.U.	target. meas.	-	-	✓	-	-	-	-	-
	O2P	✓	-	-	✓	✓	✓	-	✓
	P2P · use P2P	✓	-	-	-	-	-	-	✓
	P2P · M-P2P	✓	-	-	-	-	-	-	-
	P2P · L.P.M.	✓	-	-	-	-	-	-	-
E.S.	cost-utility	✓	✓	✓	✓	-	✓	✓	-
	POMDP	-	-	-	-	✓	-	-	✓

the observed map. Although these methods do not address exploration in the unseen space, it is meaningful in that the concept of considering the context between objects and spaces is addressed. [16] introduces the concept of attention, by approximately establishing a region of interest where the target might exist, and then generating a path towards it. [1] uses semantic information from scattered objects to infer the probability of existence of the target object. [16] and [1] both make inferences for target localization based on the observed structural context of the space. [7] and [17] adopts a partially observable Markov decision process (POMDP) for exploration decision in an unknown space to find the target and uses semantic information of places and objects. However, the region of interest is limited to the already observed space, which means the probability that the target is over a frontier is not considered.

The inference methods of unseen space to speed up the robot exploration are also proposed. [19] proposes the use of a TSP solver by assuming that prior map information in the form of topo-metric graph is available. Although the topo-metric graph that corresponds to the mission environment is needed, it is worthwhile to refer to in that unknown space over frontiers is inferred in the scenario. [21], [23] and [24] use a Deep Neural Network (DNN) to predict the local unseen space around frontiers to speed up the exploration. [20] adopts the Gaussian Process (GP) to predict the potential value of the goals to maximize the spatial information gain. [19], [21], [24] and [20] use predicted space information to explore the map efficiently, but they only consider the volumic information maximization.

[25] and [6] utilize the concept of space inference and object-to-space (O2S) relation knowledge to efficiently guide robot to a probable location to find the target. They first abstract the map to the graph domain and the space-to-space (S2S) relation based space inference is performed by leveraging on the indoor floorplan dataset; however, these methods do not consider complex relations in which more than two spaces are interconnected, or the counting based heuristic algorithm without using the latent pattern cognitive model is not promising to understand the context of indoor semantic-spatial relations.

B. SEMANTIC PERCEPTION AND NAVIGATION

In addition to studies directly related to robot exploration missions (section II-A), this subsection describes overall studies related to the semantic perception and robot navigation using it. Many robot navigation problems consider the interaction with the external environment [26]–[28]. In particular, the semantic representation of the environment (e.g., room number, objects, functional category of roads or spaces) contains valuable information for missions. To exploit the semantic information, the semantic mapping methods using a camera [29]–[34], or multiple heterogeneous sensors [35], [36] are proposed. Also, the usability of the semantic perception methods have been increased due to the public map datasets [5], [37]. The datasets contain semantic information about outdoor or indoor environments. [38] and [28] suggest global outdoor navigation method by matching the robot sensing data with the OpenStreetMap data using geometric and semantic features. Similarly, in the indoor navigation, robot navigation methods comparing the geometric and semantic sensing data with given flooplan data are suggested [39]–[42]. With the advances of the semantic perception, navigation methods, and public navigational datasets, pattern-cognitive navigation is promising.

C. GRAPHICAL MAP ABSTRACTION

Graph abstraction has been developed for various purposes in various fields, and attempts have been made to abstract indoor space into graphs in fields such as robotics and geometry. Many of robot exploration problems also adopt the graphical map abstraction technique for an efficient inference on spaces [1]–[7]. The location and connection of nodes are determined by various perspectives, including inter-visibility [43]–[45], sampling [41], [42], [46], and spatial segmentation methods [47], [48]. Among these, this paper uses the voronoi-based graph generation method that performs the graph extraction by spatial segmentation methods [47].

D. MULTIVARIATE BERNOULLI DISTRIBUTION MODEL

We consider the inference of the existence and category of unknown nodes beyond the node of interest with the graph obtained by abstracting partially observed map as input. It is known that MBD model can efficiently

represent the distribution of the multivariate Bernoulli graph by capturing high-order interactions of multiple groups of nodes as well as relationships between two variables. Also, the categorical graph, which is the same format with semantic-spatial relation data can be represented by generalizing Bernoulli (Binary) random variables. A method to optimize the latent parameters in MBD model using linear predictors is proposed in [49]. [50] considers a multivariate Bernoulli model that uses a smoothing spline model to replace the linear predictor, but setting the second and higher order interactions between the nodes as constants. [51] and [52] try to build a unified framework of a generalized linear model for the multivariate Bernoulli distribution which includes both higher order interactions among the nodes and covariate information. [53] and [54] suggest a deep neural network-based parameter learning method using the MBD. Existing studies show that MBD models have the ability to capture the context of graphs with discrete variables, and focus on learning them by high-order parameterization.

According to these studies, we discover that pattern cognitive learning model for space inference and non-myopic target-directed exploration problem has not been properly investigated. Motivated by the graphical map abstraction concept and the characteristics of MBD models learning interactions between discrete nodes, we propose the graphical space inference model and the target-directed exploration planner aided by it.

III. PROBLEM STATEMENT

Consider a mobile robot that operates in a closed 2D indoor environment $M \in \mathcal{M}^{w \times h}$, incrementally building an estimated map $\hat{M} \in \mathcal{M}^{w \times h}$, in which $\mathcal{M} \in \{\mathcal{O} : \text{occupancy}, \mathcal{C} : \text{functional category of space}\}$ is map configuration, $\mathcal{O} \in \{F : \text{free}, O : \text{occupied}, U : \text{unknown}\}$ is configuration of cell occupancy, $\mathcal{C} \in \{1, \ldots, N_c\}$ is category of cell, and w and h are the maximum width and height of map, respectively. For efficient target search in unknown environments, we present an exploration framework that generates goals in the direction of maximizing the detection probability of the target while reducing the overall cost of travel until the target is found:

$$\max_X \left(p_{\psi(X)}(o_t) - C(X) \right) \quad (1)$$

where X is the traveled trajectory, $C(\cdot)$ is the cost, $\psi(X) = \hat{M}_O \bigcup \hat{M}_F$ is observed space by the travel X, $o_t \in \{0, 1\}$ is existence of target, and $p_\psi(o_t)$ is the target existence probability in the space ψ. To deal with the cost $C(X)$ and utility $p_\psi(o_t)$ jointly, it is necessary to infer the existence of a target in unobserved spaces. To incorporate the inference concept and the exploratory target search problem, we define several probabilities related to space and objects as follows:

- $p(E_{c_j}^{o_t}) \in [0, 1]$: The existence probability of target in a space in category c_j
- $p(H_{x_j}^{c_i}) \in [0, 1]$: The probability that the category of hypothetical space over space x_j is c_i

To handle the objective (equation 1) in the cost-utility-based frontier exploration manner, the following

Exploration-Search Transform (EST) concept is suggested. The EST generates a cost-utility map $\theta(x) \ \forall x \in \hat{\mathcal{M}}$. In the cost-utility map, the shortest path from an initial robot position to the best next goal in frontiers can be extracted by simply following the steepest gradient. The value of each cell in the cost-utility map is defined as follows:

$$\theta(x) = \max_{x_f \in \mathcal{F}} \left[\max_{X \in \mathcal{X}_x^{x_f}} \left(C(X) \right) - \beta V_M(\hat{M}, x_f) \right] \quad (2)$$

$$V_M(\hat{M}, x_f) = \sum_{c_j=1}^{N_c} p(E_{c_j}^{o_t}) p(H_{x_f}^{c_j} | \hat{M})$$

$$+ \gamma \sum_{c_j=1}^{N_c} p(E_{c_j}^{o_t}) \sum_{\bar{x}_{f1}=1}^{N_c} p(H_{\bar{x}_{f1}}^{c_j} | \bar{M}_{x_f}^{\bar{x}_{f1}})$$

$$+ \cdots$$

$$+ \gamma^{R-1} \sum_{c_j=1}^{N_c} p(E_{c_j}^{o_t}) \sum_{\bar{x}_{fR-1}=1}^{N_c}$$

$$\cdots \sum_{\bar{x}_{f2}=1}^{N_c} \sum_{\bar{x}_{f1}=1}^{N_c} p\left(H_{\bar{x}_{fR-1}}^{c_j} | \bar{M}_{v_f}^{\bar{x}_{f1}, \cdots, \bar{x}_{fR-1}} \right) \quad (3)$$

where $\mathcal{F}$ is the set of all frontiers in $\hat{M}$, $\mathcal{X}_x^{x_f}$ is the set of all paths from x to x_f, $C(X)$ is the cost of path X, $V_M(\hat{M}, x_f)$ is the value of the frontier x_f, γ is the discounting factor (set to 0.99), $p(H_{\bar{x}_{fk}}^{c_j} | \bar{M}_{x_f}^{\bar{x}_{f1}, \cdots, \bar{x}_{fk}})$ is the probability that the category of hypothetical space over space $\bar{x}_{fk}$ turns out to be c_j given map $\bar{M}_{x_f}^{\bar{x}_{f1}, \cdots, \bar{x}_{fk}}$, $\bar{M}_{x_f}^{\bar{x}_{f1}, \cdots, \bar{x}_{fk}}$ is the predicted map after action sequences $(x_f, \bar{x}_{f1}, \cdots, \bar{x}_{fk})$ are taken, R is the roll-out length, and α is the coefficient. To focus on space inference and planning, we introduce following assumptions:

Assumption 1: The existence probability of target in a space in category c_j $p(E_{c_j}^{o_t})$ is given in advance

Assumption 2: At the time of mapping, the probability that the category of hypothetical space over space x_j is c_i $P(C_{x_j}^{c_i})$ for all $x_j \in \hat{M}_F$ are given

In this paper, we focus on the following tasks:

- Building the space inference model to obtain $p(H_{x_f}^{c_j} | M)$
- Building the next-goal generation method aided by the space inference model

IV. GRAPHICAL SPACE INFERENCE AIDED GOAL GENERATION

Due to huge dimensionality of the state space representation of the map in the metric domain, the construction of a space inference model in that domain is also computationally intractable. Therefore, the metric domain of the environment is converted to the graph domain ((a) in Figure 1), and we redefine EST in the graphical domain as follows:

$$\theta(x) = \max_{x_f \in \mathcal{F}} \left[\max_{X \in \mathcal{X}_x^{x_f}} \left(C(X) \right) \right.$$

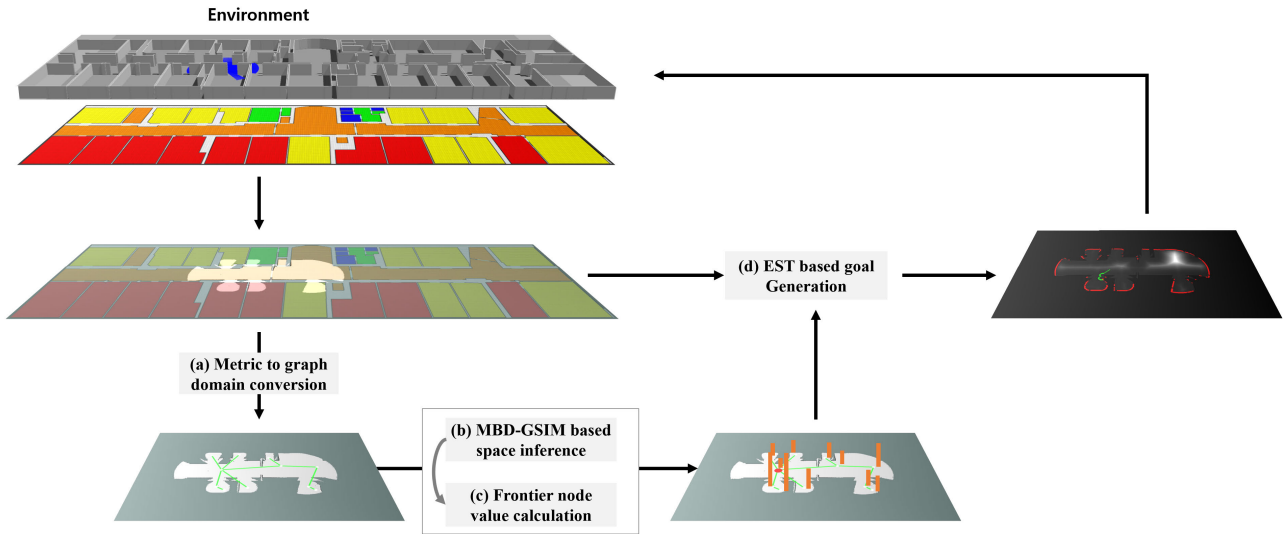$$\left. - \beta V_G \left(T_M(\hat{M}), T_V(T_M(\hat{M}), x_f) \right) \right] \quad (4)$$

Environment

FIGURE 1. Space inference aided next-goal generation.

$$
V_G(G, v_f) = \sum_{c_j=1}^{N_c} p(E_{c_j}^{o_t}) p(H_{v_f}^{c_j}|G)
$$

$$
+ \gamma \sum_{c_j=1}^{N_c} p(E_{c_j}^{o_t}) \sum_{\bar{v}_{f1}=1}^{N_c} p\left(H_{\bar{v}_{f1}}^{c_j}|\bar{G}_{v_f}^{\bar{v}_{f1}}\right)
$$

$$
+ \cdots
$$

$$
+ \gamma^{R-1} \sum_{c_j=1}^{N_c} p(E_{c_j}^{o_t}) \sum_{\bar{v}_{fR-1}=1}^{N_c}
$$

$$
\cdots \sum_{\bar{v}_{f2}=1}^{N_c} \sum_{\bar{v}_{f1}=1}^{N_c} p\left(H_{\bar{v}_{fR-1}}^{c_j}|\bar{G}_{v_f}^{\bar{v}_{f1},\cdots,\bar{v}_{fR-1}}\right) \quad (5)
$$

where $T_M(\cdot) : \mathcal{M} \to \mathcal{G}$ is the conversion function from a metric map to a converted graph, $T_V(\cdot) : \mathcal{G} \times \mathbb{R}^2 \to v$ is the conversion function from a metric position to a closest node in the converted graph G, $p\left(H_{\bar{v}_{fk}}^{c_j}|\bar{G}_{v_f}^{\bar{v}_{f1},\cdots,\bar{v}_{fk}}\right)$ is the probability that the category of hypothetical node over node $\bar{v}_{fk}$ is c_j given graph $\bar{G}_{v_f}^{\bar{v}_{f1},\cdots,\bar{v}_{fk}}$. The graph representation G is defined as follows:

$$
G = (\mathcal{V}, \mathcal{E}, \mathcal{W}) \quad (6)
$$

where $\mathcal{V}$ is a set of nodes, $\mathcal{E} \subseteq (\mathcal{V} \times \mathcal{V})$ is a set of edges, and $\mathcal{W} \in \{\mathcal{P}, \mathcal{C}, \mathcal{I}_f, \mathcal{I}_r\}$ is the set of node features. In the node features, $\mathcal{C} \in \{c_1, \cdots, c_{N_c}\}^{|\mathcal{V}|}$ is the category set of nodes, $\mathcal{P} \in \mathbb{R}^{|\mathcal{V}| \times 2}$ is a position set of nodes, $\mathcal{I}_f \in \{0, 1\}^{|\mathcal{V}|}$ is the vector of indicator function, which equals 1 if any frontier is near the node and 0 otherwise, and $\mathcal{I}_r \in \{0, 1\}^{|\mathcal{V}|}$ is also the vector of indicator function that equals 1 if the robot is at the node and 0 otherwise.

Among the information in the graph, $(\mathcal{V}, \mathcal{E}, \mathcal{C})$ which contains semantic categories of space and their relations are used for MBD-GSIM. In the model learning phase of
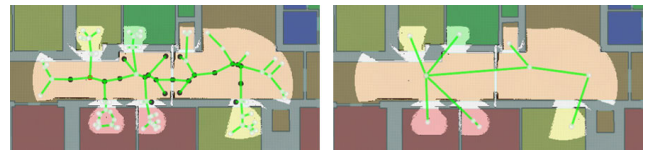

FIGURE 2. Example of metric to graph domain conversion (left:GVD [47], right:RGVD (algorithm 1)).

MBD-GSIM, the semantic-spatial relations in the graph dataset are exploited, and in the prediction phase, the space beyond the node of interest in the graph $p\left(H_{\bar{v}_{fk}}^{c_j}|\bar{G}_{v_f}^{\bar{v}_{f1},\cdots,\bar{v}_{fk}}\right)$ is inferred by using the graph and the node of interest as the inputs ((c) in Figure 1). The space inference information is used to calculate the frontier node values $V_G\left(T_M(\hat{M}), T_V(T_M(\hat{M}), x_f)\right)$ ((b) in Figure 1) using Equation 5. Based on the frontier values, the next goal is extracted ((d) in Figure 1) by following the steepest gradient from the current robot position in the cost-utility map derived from Equation 4.

In this paper, we use the Generalized Voronoi Diagram (GVD) scheme [47] for metric to graph domain conversion. A Voronoi diagram can be considered as a collection of the medial axes between a set of points. The graph G from GVD can be considered as the medial lines between the obstacles, which can be used to form an indoor representative graph. To generate the graph, because the GVD scheme considers only the geometric features to generate the graph, it has many redundant nodes in the paths between free spaces. For the semantic space inference we intend to perform in this paper, it is better to represent the space considered semantically identical as one node. For that, a reduced GVD scheme (Algorithm 1, Figure 2) is suggested. It utilizes the node category information and betweenness centrality concept to merge the nodes without losing the adequacy of the geometric placement of the nodes.

Algorithm 1 Reduced GVD

1: **Input:** map $\hat{M}$, maximum number of nodes in each cluster N_g
2: Obtain G using GVD scheme [47] with input $\hat{M}$
3: **for all** $c_i \in \{1, \cdots, N_c\}$ **do**
4: $\quad \mathbf{G}_{c_i} \leftarrow$ {connected subgraphs in G of category c_i}
5: $\quad$ **while** $\exists |G^s_{c_i}| > N_g$ in $\mathbf{G}_{c_i}$ **do**
6: $\quad\quad$ **for all** $G^s_{c_i} \in \mathbf{G}_{c_i}$ **do**
7: $\quad\quad\quad$ **if** $|G^s_{c_i}| > N_g$ **then**
8: $\quad\quad\quad\quad \mathbf{e} \leftarrow$ {acyclic edges in $G^s_{c_i}$}
9: $\quad\quad\quad\quad e_r \leftarrow argmax_{e \in \mathbf{e}}$(betweeness centrality of e)
10: $\quad\quad\quad\quad \mathcal{E}^s_c \leftarrow \mathcal{E}^s_c \setminus e_r$
11: $\quad\quad\quad\quad \mathbf{G}_{c_i} \leftarrow$ {connected subgraphs
12: $\quad\quad\quad\quad\quad\quad\quad$ with category c_i in G}
13: $\quad\quad\quad$ **end if**
14: $\quad\quad$ **end for**
15: $\quad$ **end while**
16: $\quad$ **for all** $G^s_{c_i} \in \mathbf{G}_{c_i}$ **do**
17: $\quad\quad$ merge nodes
18: $\quad$ **end for**
19: **end for**
20: **Return:** G

V. MBD-GSIM BASED SPACE INFERENCE

In this section, we describe the MBD-GSIM. MBD-GSIM infers the semantic category of space beyond the node of interest $p(H^{c_i}_{v_f}|G)$. For this, the concept of MBD model (section V-A), and MBD-GSIM scheme (section V-B) based on it are described.

A. MULTIVARIATE BERNOULLI DISTRIBUTION MODEL

MBD is suitable for modeling graphs of Bernoulli nodes with the concept of statistical correlations. The K-dimensional random vector and its realization are defined as follows:

$$\mathbf{Y} = (Y(1), Y(2), \cdots, Y(K))$$
$$\mathbf{y} = (y(1), y(2), \cdots, y(K)) \quad (7)$$

where $\mathbf{Y}(i)$ $\forall i \in \{1, \cdots, K\}$ are the possibly correlated Bernoulli random variables (nodes), and K is the number of the bernoulli nodes. The joint probability distribution of $\mathbf{y}$ is as follows:

$$p(\mathbf{y}) = p_{0,0,\cdots,0}^{\prod_{j=1}^{K}(1-y(j))} \, p_{1,0,\cdots,0}^{y(1)\prod_{j=2}^{K}(1-y(j))}$$
$$\cdot p_{0,1,\cdots,0}^{(1-y(1))y(2)\prod_{j=3}^{K}(1-y(j))} \cdots p_{1,1,\cdots,1}^{\prod_{j=1}^{K}y(j)} \quad (8)$$

where $p_{y_1,y_2,\cdots,y_K} = p(y(1), y(2), \cdots, y(K))$. For simplification, the following definition is introduced:

Definition 1: For any two superscripts $\tau_1 = \{j_1, j_2, \ldots, j_r\}$ such that $\tau_1 \in \mathcal{T}$ and $\tau_2 = \{k_1, k_2, \ldots, k_s\}$ with $\tau_2 \in \mathcal{T}$ and $r \leq s$, we can say that $\tau_1 \subseteq \tau_2$ if for any $j \in \tau_1$, there is a $k \in \tau 2$ such that $j = k$, where $\mathcal{T}$ is the power set of indices $\{1, 2, \ldots, K\}$.

Using Equation 8 and Definition 1, log-linear formulation $l(\mathbf{y}, \mathbf{f}(\mathbf{x}))$ can be written as follows:

$$l(\mathbf{y}, \mathbf{f}(\mathbf{x})) = -log[p(\mathbf{y})]$$
$$= -\sum_{\tau \in \mathcal{T}} f^\tau(\mathbf{x})B^\tau(\mathbf{y}) + b(\mathbf{f}(\mathbf{x}))$$
$$B^\tau(\mathbf{y}) = \prod_{j \in \tau} y(j)$$
$$b(\mathbf{f}(\mathbf{x})) = log\left[1 + \sum_{\tau \in \mathcal{T}} exp[S^\tau(\mathbf{x}(i))]\right]$$
$$S^\tau = \sum_{\tau_0 \subseteq \tau} f^{\tau_0}(\mathbf{x}) \quad (9)$$

where $\mathcal{T}$ is the set of all possible subsets of $\{1, 2, \cdots, K\}$, and $\mathbf{f} = (f^{\{1\}}, f^{\{2\}}, \cdots, f^\tau, \cdots, f^{\{1,2,\cdots,K\}})$ is the vector of the natural parameters. $\mathbf{x} \in \mathbb{R}^p$ is the input feature vector, and $y \in \mathbb{I}^K$ is the realization of the multivariate Bernoulli random vector. The natural parameter $f^\tau(\mathbf{x})$ represents the interaction between nodes belonging to τ, and it is to be fitted by training. Given the N_d data pairs $\mathbf{x}^i = (x^i(1), .., x^i(p))$, $\mathbf{y}^i = (y^i(1), , , y^i(K))$ $\forall i \in \{1, \cdots, N_d\}$, equation 9 is rewritten as follows:

$$l(\mathbf{y}, \mathbf{f}(\mathbf{x})) = \frac{1}{N_d}\sum_{i=1}^{N_d}\left[-\sum_{\tau \in \mathcal{T}} f^\tau(\mathbf{x}^i)B^\tau(\mathbf{y}^i) + b(\mathbf{f}(\mathbf{x}))\right] \quad (10)$$

Fitting f^τ $\forall \tau \in \mathcal{T}$ using equation 10 can be said to be the construction of an MBD model. Once the model is constructed, it is possible to calculate the joint probability of $\mathbf{y}$ by the following formula:

$$p(\mathbf{y}^\tau) = \frac{(exp(S^\tau(x)))}{(1 + \sum_{\tau \in \mathcal{T}} exp[S^\tau(x)])} \quad (11)$$

where $p(\mathbf{y}^\tau) = P(Y(i) = 1 \; \forall i \in \tau, Y(j) = 0 \; \forall j \notin \tau)$. One example of computing the joint probability of multivariate Bernoulli random variables using trained $f^\tau(x)$ is as follows:

$$P(Y(1) = 1, Y(2) = 1, Y(3) = 0)$$
$$= \frac{exp(S^{\{1,1,0\}}(x))}{1 + S^{\{0,0,0\}} + S^{\{1,0,0\}} + \cdots + S^{\{1,1,1\}}}$$
$$S^{\{0,0,0\}} = f^{\{0,0,0\}}(x)$$
$$S^{\{1,0,0\}} = f^{\{0,0,0\}}(x) + f^{\{1,0,0\}}(x)$$
$$S^{\{0,1,0\}} = f^{\{0,0,0\}}(x) + f^{\{0,1,0\}}(x)$$
$$\cdots$$
$$S^{\{1,1,1\}} = f^{\{0,0,0\}}(x) + f^{\{1,0,0\}}(x) + \cdots + f^{\{1,1,1\}}(x) \quad (12)$$

where x is the input feature vector, and $f^{\{k_1,k_2,k_3\}}$ $(k_i \in \{0, 1\})$ is the natural parameter. Using the concept of MBD, we build MBD-GSIM which takes a graph of a partially observed map as a query and output predicted space information.

B. MBD-GSIM

Figures 3 illustrates the MBD-GSIM and its training framework, respectively. In the training phase (Figure 3-(b)),
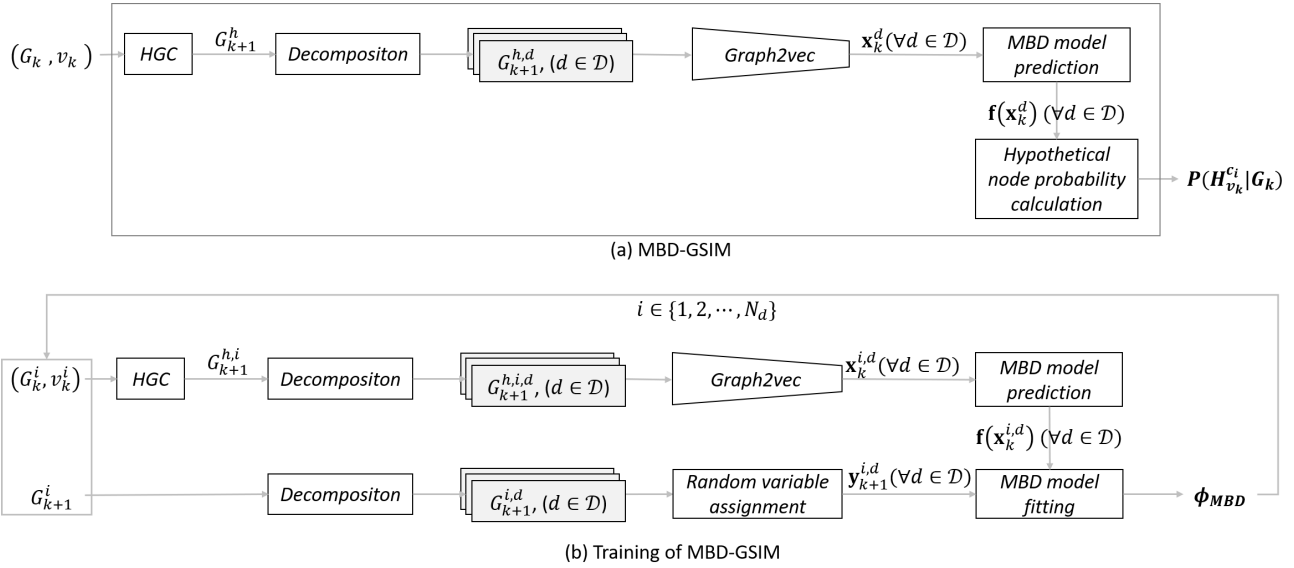
FIGURE 3. MBD-GSIM (a) and it's training phase (b).

the N_d datapairs are given as follows:

$$(\text{query}^i, \text{label}^i) = ((G_k^i, v_k^i), G_{k+1}^i), \quad i = 1, 2, \cdots, N_d$$

$$(13)$$

(G_k^i, v_k^i) is the graph and the node of interest and G_{k+1}^i is the resulting graph when the action of taking v_k^i is taken. k and $k+1$ are used as notations to distinguish between the query and the label data, respectively. In this paper, we generate the data pairs from the graph format KTH dataset [5] (examples are in the Figure 4) through random walk exploration (Figure 5).

The MBD model takes a real-valued feature vector and Bernoulli (binary) multivariate vector for the input and realization, respectively. However, the dataset is given in the form of the graph and the index of the node (Equation 13). Because the required data format of the MBD model $(\mathbf{x}_k^i, \mathbf{y}_{k+1}^i)$ and given dataset (Equation 13) do not match, some conversion functions between them are needed. First, the 'Hypothetical Graph Construction (HGC)' makes the query (G_k^i, v_k^i) into a single hypothetical graph $G_{k+1}^{h,i}$. Then, the 'Decomposition' module decomposes $G_{k+1}^{h,i}$ and G_{k+1}^i into multiple path graphs as a preprocessing to vectorize them. After that, the decomposed data pairs $(G_{k+1}^{h,i,d}, G_{k+1}^{i,d}) \, \forall d \in \mathcal{D}$ are encoded into vector form $(\mathbf{x}_k^{i,d} \, \mathbf{y}_{k+1}^{i,d}), \forall d \in \mathcal{D}$ through the 'Graph2vec' (for $G_{k+1}^{h,i,d}$) and 'Random Variable Assignment (RVA)' (for $G_{k+1}^{i,d}$). Based on the data pairs $(\mathbf{x}_k^{i,d}, \mathbf{y}_{k+1}^{i,d})$, the model ϕ_{MBD} is trained.

The trained MBD-GSIM (Figure 3-(a)) only requires (G_k, v_k) as an input. Like the training phase, x_k^d is obtained through 'HGC', 'Decomposition', and 'Graph2vec'. With the feature vector input $x_k^d \, \forall d \in D$, the MBD model outputs natural parameter $f^\tau(x_k^d) \, \forall d \in D$, which is used to obtain 'Hypothetical node probability calculation'. In the following subsections, each module in Figure 3 are described.
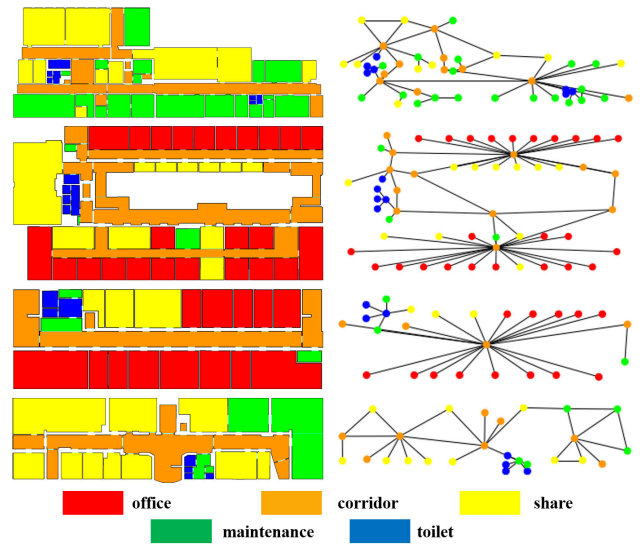

FIGURE 4. Example of KTH dataset (left: Floorplan color-coded according to semantic categories, right: Graph representation of the floorplans).

1) HYPOTHETICAL GRAPH CONSTRUCTION

HGC is the process of constructing one hypothetical graph representation G_{k+1}^h by integrating the original query (G_k, v_k). Starting from the graph $G_k = (\mathcal{V}_k, \mathcal{E}_k, \mathcal{C}_k)$, G_{k+1}^h is derived as follows:

$$G_{k+1}^h = (\mathcal{V}_{k+1}^h, \mathcal{E}_{k+1}^h, \mathcal{C}_{k+1}^h)$$
$$\mathcal{V}_{k+1}^h = \mathcal{V}_k \cup v_{k+1}^h$$
$$\mathcal{E}_{k+1}^h = \mathcal{E}_k \cup (v_k, v_{k+1}^h)$$
$$\mathcal{C}_{k+1}^h = \mathcal{C}_k \cup \{0\} \qquad (14)$$

where v_{k+1}^h is a newly defined hypothetical node. The neighbor node of v_{k+1}^h is set to the node of interest v_k. Because
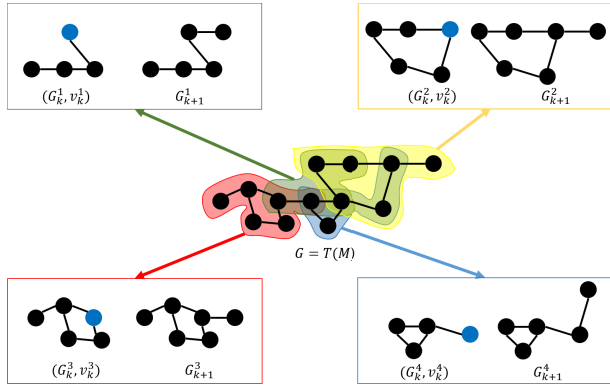
FIGURE 5. Example of random-walk based dataset generation: The prior map graph G_k^i is set by random initial start and random walks. The blue node is the node of interest (v_k^i) in G_k^i, which is selected randomly. With the query (prior) (G_k^i, v_k^i), the label G_{k+1}^i is obtained from the ground truth graph $G = T(M)$.
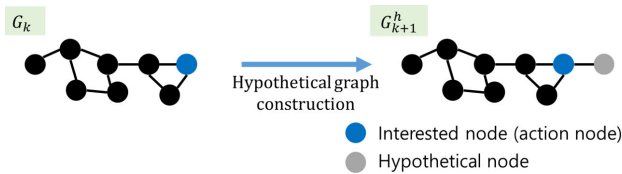

FIGURE 6. Example of hypothetical graph construction.

the existence and category of v_{k+1}^h is uncertain, it is assigned a dummy category 0. The example of HGC is shown in the Figure 6.

2) DECOMPOSITION

In MBD-GSIM training, the label graph G_{k+1}^i of data pair ($G_{k+1}^{h,i}$, G_{k+1}^i) should be represented as a multivariate Bernoulli variable. However, the multivariate Bernoulli variable cannot be obtained directly from G_{k+1}^i because the graph format does not naturally have priorities between nodes, but it may contain cycle subgraphs, has unlimited size, and the structure changes at every step. Therefore, we introduce the assumptions below to decompose the graph G_{k+1}^i into map-pable form to the multivariate bernoulli variable.

Assumption 3: Structural features of indoor graph G can be approximated with BFS tree graph G'.

Assumption 4: The characteristic of the place of interest can be captured through the context of the nearby surrounding places.

Assumption 5: The spatial properties of the tree graphs can be expressed as a set of path graphs from root nodes to all leaf nodes.

With the above assumptions, we propose a graph decomposition process as shown in Figure 7. First, with assumption 3, we extract the BFS tree by setting the hypothesis node as the root node. Then, because the large graph sizes can makes training and prediction computationally intractable, the depth of the tree is limited to the length L set by user. Assumption 4
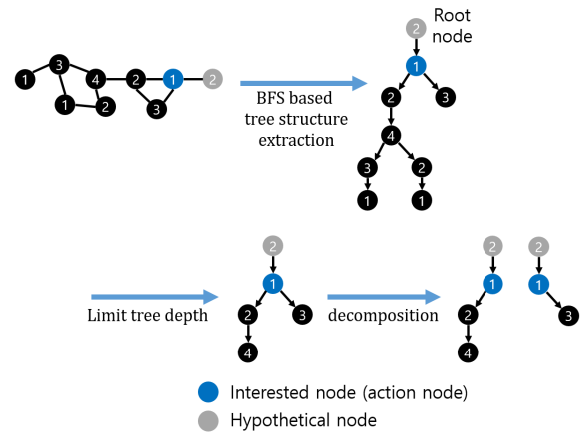

FIGURE 7. Example of indoor graph decomposition.

allows us to limit the input size by considering only the space within a certain range around the node of interest. Finally, we obtain a set of path graphs ($G_{k+1}^{h,i,d}$, $G_{k+1}^{i,d}$) $\forall d \in \mathcal{D}^i$ that connect all leaf nodes to the root node (assumption 5).

3) Graph2vec

We construct the graph embedding model to obtain the input feature $\mathbf{x}_k^d$ $\forall d \in \mathcal{D}$ for the downstream MBD model. For that, we apply the widely adopted Graph2vec [55] scheme which provides δ-dimensional distributed representations for the given graph dataset. Given the decomposed path graphs $G_{k+1}^{h,i,d}$ ($\forall i \in \{1, \cdots, N_d\}, d \in \mathcal{D}^i$), the optimal embedding model for downstream MBD model is obtained by the following objective function:

$$\sum_{j=1}^{|\mathcal{D}^i|} log(P(sg^j|G^i)) \tag{15}$$

where $P(sg^j|G^i)$ is defined as,

$$\frac{exp(G^i \cdot sg^j)}{\sum_{sg \in \mathcal{SG}} exp(G^i \cdot sg)} \tag{16}$$

and $\mathcal{SG}$ is the set of all the subgraphs across all path graphs.

The overall process to construct the graph embedding model using query dataset $\{(G_k^i, v_k^i)|\forall i \in \{1, \cdots, N_d\}\}$ is shown in algorithm 2. For all queries, 'HGC' (line 5) and 'Decomposition' (line 6) are applied, and the decomposed hypothetical graph sets $G_{k+1}^{h,d}$ are gathered to construct the graph embedding model (line 7). The typical Graph2vec optimizer is applied to construct the embedding model ϕ with Equation 15 as the objective function (lines 9~18).

4) RANDOM VARIABLE ASSIGNMENT

RVA is the operation of assigning the decomposed label data $G_{k+1}^{i,d}$ to a multivariate Bernoulli (binary) vector as follows (hot-encoding for each node):

$$\mathbf{y}_{k+1}^{i,d} = [vec(G_{k+1}^{i,d}(1)), vec(G_{k+1}^{i,d}(2)), \cdots, vec(G_{k+1}^{i,d}(L))] \tag{17}$$

Algorithm 2 Graph Embedding Model Construction

1: **Input:** Query dataset $\{(G_k^i, v_k^i)|\forall i \in \{1, \cdots, N_d\}\}$, length limit of graph L, number of epochs N_e, maximum degree of rooted subgraphs D, learning rate α
2: **Initialize:** Graph2vec embedding model ϕ_{G2V}
3: $\mathbf{G}^E = \{\}$
4: **for all** $i = 1$ **to** N_d **do**
5:     $G_{k+1}^h \leftarrow HGC(G_k^i, v_k^i)$
6:     $\mathbf{G}_{k+1}^{h,d} \leftarrow Decomposition(G_{k+1}^h, v_{k+1}^h, L)$
7:     $\mathbf{G}^E \leftarrow \mathbf{G}^E \cup \mathbf{G}_{k+1}^{h,d}$
8: **end for**
9: **for all** $e = 1$ **to** N_e **do**
10:     $\mathbf{G}^E = Shuffle(\mathbf{G}^E)$
11:     **for all** $G^i \in \mathbf{G}^E$ **do**
12:         $\mathcal{SG} \leftarrow Getsubgraphs(G^i)$
13:         **for all** $sg^j \in \mathcal{SG}$ **do**
14:             $J(\phi_{G2V}) = -logP(sg^j|\phi_{G2V}(G^i))$
15:             $\phi_{G2V} \leftarrow \phi_{G2V} - \alpha \frac{\partial J}{\partial \phi_{G2V}}$
16:         **end for**
17:     **end for**
18: **end for**
19: **Return** ϕ_{G2V}

Algorithm 3 Training

1: **Input:** (Query, label) dataset $\{((G_k^i, v_k^i), G_{k+1}^i)|\forall i \in \{1, \cdots, N_d\}\}$, length limit of graph L, graph embedding model ϕ_{G2V}
2: **Initialize:** MBD model ϕ_{MBD}
3: $\mathbf{G}^Q = \{\}$
4: $\mathbf{G}^L = \{\}$
5: **for all** $i = 1$ **to** N_d **do**
6:     $G_{k+1}^h = HGC(G_k^i, v_k^i)$
7:     $\mathbf{G}_{k+1}^{h,d} = Decomposition(G_{k+1}^h, v_{k+1}^h, L)$
8:     $\mathbf{G}_{k+1}^d = Decomposition(G_{k+1}, v_{k+1}^h, L)$
9:     $\mathbf{G}^Q = \mathbf{G}^Q \cup \mathbf{G}_{k+1}^{h,d}$
10:     $\mathbf{G}^L = \mathbf{G}^L \cup \mathbf{G}_{k+1}^d$
11: **end for**
12: $\mathcal{X} = \{\}$
13: $\mathcal{Y} = \{\}$
14: **for all** $(G^Q, G^L) \in (\mathbf{G}^Q, \mathbf{G}^L)$ **do**
15:     $\mathbf{x} = \phi_{G2V}(G^Q)$
16:     $\mathbf{y} = RVA(G^L)$
17:     $\mathcal{X} = \mathcal{X} \cup \{\mathbf{x}\}$
18:     $\mathcal{Y} = \mathcal{Y} \cup \{\mathbf{y}\}$
19: **end for**
20: Fit ϕ_{MBD} by Equation 10 with input $\mathcal{X}$ and $\mathcal{Y}$
21: **Return** ϕ_{MBD}

---

where $vec(\cdot)$ is the hot-encoding operation, $G_{k+1}^{i,d}(1)$ is the hypothetical node, and $G_{k+1}^{i,d}(L)$ is the leaf node. Here, since the node information is not binary but categorical information of nodes, N_c variables for each node are required, and the number of variables required increases linearly with maximum length L of the path graph from the hypothetical node considered. If it is determined that there is a wide range of surrounding spaces affecting the node of interest to be inferred, then L can be increased, and vice versa.

The generated vector-type (query, label) dataset is used to fit the MBD model using Equation 10. The overall training process, including previous processes from the query and label input, is described in algorithm 3. The original dataset is encoded to the required form for MBD model (line 3 ~ 19), then the natural parameter predictor ϕ_{MBD} is fitted.

5) HYPOTHETICAL NODE PROBABILITY CALCULATION

Using the trained model ϕ_{MBD}, the following natural parameters can be obtained:

$$f^\tau(\mathbf{x}^d) \ \forall \tau \in \mathcal{T}, \ d \in \mathcal{D} \quad (18)$$

The predicted natural parameter $f^\tau(\mathbf{x}^d) \ d \in \mathcal{D}$ is used to calculate the joint probability $p(\mathbf{y}^\tau) = P(Y(i) = 1 \ \forall i \in \tau, Y(j) = 0 \ \forall j \notin \tau)$ which represents the existence and category probability of a hypothetical node. For the calculation, followings are considered:

1) We are interested in the hypothetical node, so it is necessary to marginalize the above joint probability for the hypothetical node related random variables.
2) Since $\mathbf{f}(X) = \{\mathbf{f}(\mathbf{x}^d)|\mathbf{x}^d \ \forall d \in \mathcal{D}\}$ is a natural parameter prediction for the decomposed query input,

a mechanism for recombining predicted probability information is needed.

For the first consideration, the variables associated with the hypothetical node in multivariate Bernoulli random vector $\mathbf{Y} \in \mathbf{1}^{N_c \cdot L}$ are the $1 \sim N_c$-th elements, $\mathbf{Y}(1 : N_c)$, so the marginal probabilities of the decomposed query inputs are calculated as follows:

$$p(\mathbf{y}^d(1 : N_c))$$
$$= \sum_{\forall \mathbf{y}^d(N_c+1:N_c \cdot L)} p(\mathbf{y}^d(1 : N_c), \mathbf{y}^d(N_c + 1 : N_c \cdot L)) \quad (19)$$

For the second consideration, we perform the following linear combinations of the marginal probability $p(\mathbf{y}^d(1 : N_c) \ \forall d \in \mathcal{D}$ using the decomposed query information. where α^d is the weight.

$$p(\mathbf{y}(1 : N_c)) = \sum_{d=1}^{|\mathcal{D}|} \alpha^d p(\mathbf{y}^d(1 : N_c)) \quad (20)$$

For convenience, we denote the probability variable vectors of the hypothetical node and their realizations, $\mathbf{Y}(1 : N_c)$ and $\mathbf{y}(1 : N_c)$, as $\mathbf{Y}^h$, $\mathbf{y}^h$. With the marginal probability above, the probability that the category of hypothetical place over place x_j equals c_i, $p(H_{v_k}^{l_i}|G_k)$, is defined as follow:

$$p(H_{v_k^i}^{c_i}|G_k) = P(Y^h(i) = 1, \mathbf{Y}^h(\mathcal{J}) = 0|G_k, v_k) \quad (21)$$

where $\mathcal{J} = \{j|j \in \{1, \cdots, N_c\} \& j \neq i\}$. The overall process of predicting the category of hypothetical space node is described in algorithm 4.

Algorithm 4 Overall MBD-GSIM Process

1: **Input:** Query data (G_k, v_k), length limit of graph L, graph embedding model ϕ_{G2V}, MBM model ϕ_{MBM}
2: $G_{k+1}^h = HGC(G_k, v_k)$
3: $\mathbf{G}_{k+1}^{h,d} = Decomposition(G_{k+1}^h, v_{k+1}^h, L)$
4: **for all** $G \in \mathbf{G}_{k+1}^{h,d}$ **do**
5:      $\mathbf{x} = \phi_{G2V}(G)$
6:      $X = X \cup \{\mathbf{x}\}$
7: **end for**
8: $\mathbf{f}(X) \leftarrow \phi_{MBD}(X)$
9: **for all** $\mathbf{f}(\mathbf{x}^d) \in \mathbf{f}(X)$ **do**
10:      **for all** $f^\tau(\mathbf{x}^d) \in \mathbf{f}(\mathbf{x}^d)$ **do**
11:          $S^\tau \leftarrow \sum_{\tau_0 \subseteq \tau} f^{\tau_0}(\mathbf{x}^d)$
12:          $P(Y(\tau) = 1, Y(\tau^c) = 0) \leftarrow \frac{(exp(S^\tau(\mathbf{x})))}{(1+\sum_{\tau \in \mathcal{T}} exp[S^\tau(\mathbf{x})])}$
13:      **end for**
14:      $p(\mathbf{y}^{d,h}) \leftarrow \sum_{\forall \mathbf{y}^d(N_c+1:N_cL)} p(\mathbf{y}^d(1:N_c), \mathbf{y}^d(N_c + 1 : N_c \cdot L))$
15: **end for**
16: $p(\mathbf{y}^h) \leftarrow \sum_{d=1}^{|\mathcal{D}|} \alpha^d p(\mathbf{y}^{d,h})$
17: **for all** $c_i \in \{0, 1, \cdots, N_c\}$ **do**
18:      $\mathcal{J} = \{j | j \in [1, N_c] \& j \neq i\}$
19:      $p(H_{v_k}^{c_i} | G_k) \leftarrow P(Y^h(i) = 1, \mathbf{Y}^h(\mathcal{J}) = 0 | G_k, v_k)$
20: **end for**
21: **Return** $p(H_{v_k}^{c_i} | G), \quad \forall c_i \in \{1, \cdots, N_c\}$

VI. COMPUTATIONAL COMPLEXITY REDUCTION

With $p(H_v^{C_i} | G)$ calculated from MBD-GSIM and prior information $p(E_{l_j}^{o_t})$, $V_G(G_k, v_k)$ can be obtained by Equation 5. Although all the information for EST calculation (equation 4) is prepared, calculating the cost-utility values for all cells in the map is computationally expensive as the observed map size increases. So, we redefine the EST as equation 22, where the steepest gradient is applied in the graph domain first (Phase 1), and in the metric domain at the termination node (Phase 2) sequentially.

$$\theta = \begin{cases} \max\limits_{v_f \in \mathcal{V}(I_f=1)} \left[\max\limits_{X_G \in \mathcal{X}_{G,T_V(G,x)}^{v_f}} \left(C(X) \right) - \beta V_G(G, v_f) \right], & P1 \\ \max\limits_{x_f \in \mathcal{F}_L} \left[max_{X \in \mathcal{X}_{P(v_f)}^{x_f}} \left(C(X) \right) \right], & P2 \end{cases}$$
(22)

where $P1$ and $P2$ are phase 1 and 2, respectively, $G = V_G(T_M(\hat{M}))$ is the graph representation of the map $\hat{M}$, $\mathcal{X}_{G,v_0}^{v_1}$ is the set of all path graphs from v_0 to v_1, $P(v)$ is the position of node v, and $\mathcal{F}_L(v_f)$ is the set of frontiers close to the v_f.

VII. EXPERIMENT

In this section, the performances of the proposed MBD-GSIM and MBD-GSIM aided exploration planner are evaluated. For that, the dataset and environment are introduced, and the comparisons with baselines are presented.
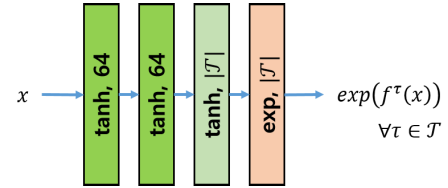

FIGURE 8. Neural network used in MBD model. This architecture takes an input vector x and outputs $exp(f^\tau)$.

TABLE 2. Accuracy improvement ratio between MBD-GSIM of $L = 1 \sim 4$ and MLP-GSIM, FSE. (L.B. and U.B. are the lower and upper bound of 3-sigma, respectively).

| | $\frac{MBD-GSIM}{MLP-GSIM} / \frac{MBD-GSIM}{FSE}$ | | | |
	$L = 1$	$L = 2$	$L = 3$	$L = 4$
L.B.	**1.27**/0.95	**1.60**/**1.19**	**1.69**/**1.26**	**1.68**/**1.25**
mean	1.00/0.93	**1.27**/**1.18**	**1.33**/**1.24**	**1.34**/**1.24**
U.B.	0.83/**1.09**	**1.07**/**1.17**	**1.11**/**1.22**	**1.12**/**1.23**

A. DATASET AND ENVIRONMENT

The KTH floorplan data of the graph form is used to train and test the MBD-GSIM (example data is shown in Figure 4-right). To train MBD-GSIM, we manually selected 20 floor plans considering the completeness of the data, and the space categories are clustered in 5 categories (office, corridor, share, maintenance, toilet). The metric form of KTH floorplan data (Figure 4-right) is also used to generate real building environments in Gazebo simulation and test the MBD-GSIM aided exploration planner in the environments. The turtlebot model equipped with a 2D LIDAR sensor and Gmapping [28] algorithm is used to build the cumulative slam map. At the time of mapping, the category of space is assumed to be given (noted in assumption 2).

B. EVALUATION METHOD

To evaluate the space inference performance of MBD-GSIM, we investigate 1) whether the MBD-GSIM learns the context of the semantic-spatial relations without overfitting, and 2) how accurate the space inference is. For that, the conventional multilayer perceptron-based GSIM (MLP-GSIM) and the Functional Subgraph Exploitation [5]-based GSIM (FSE-GSIM) are used as baselines. The neural network architecture in Figure 8 is set as the natural parameter models in MBD-GSIM.

MLP-GSIM directly outputs the space category prediction by the neural network architecture of Relu(m)-Relu(m)-Softmax(N_c), where m is the number of hidden neurons. The FSE is a representative probabilistic method using pattern matching to predict the space based on the dataset. We present the logs of loss history over training episodes to investigate whether the overfitting occurs. The loss history is compared with the MLP-GSIM. Since FSE-GSIM is a heuristic algorithm, it is not used for the overfitting comparisons. The space inference accuracy of MBD-GSIM is compared with MLP-GSIM and FSE-GSIM. The overall evaluation
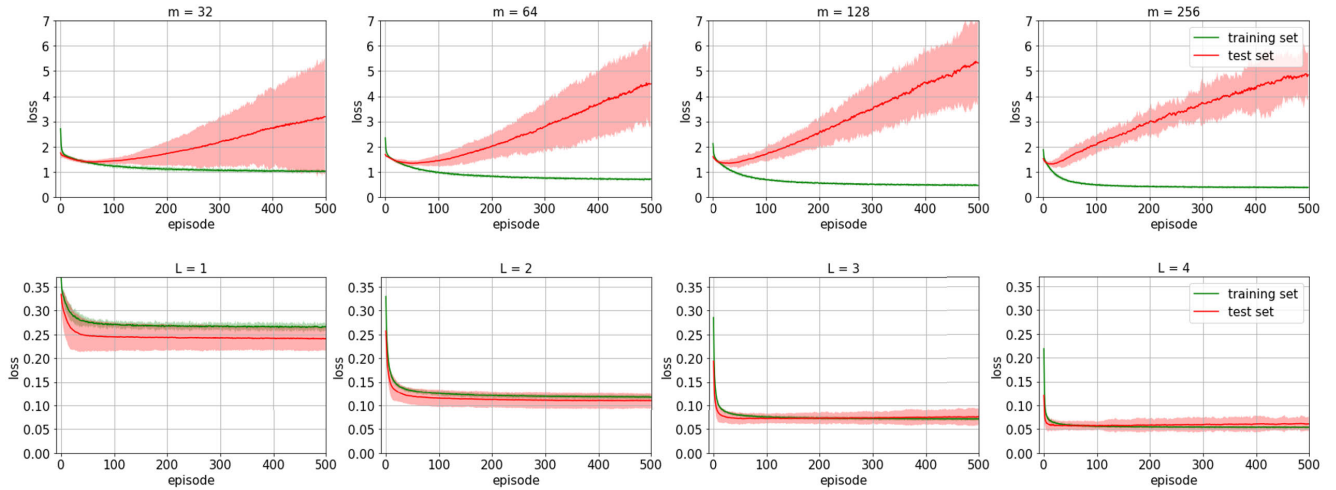
FIGURE 9. Loss history over episodes for MLP-GSIM (upper graphs) and our MBD-GSIM (lower graphs). Solid lines represent means of losses and shadows represent 3-sigma bounds. *m* is the size of hidden layers of MLP and *L* are the limit lengths of BFS for MBD-GSIM.
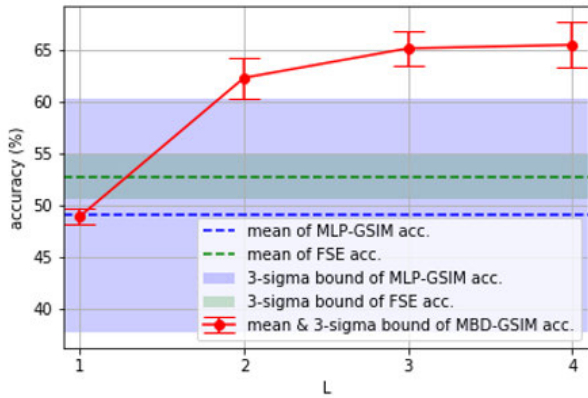

FIGURE 10. Space inference accuracy of MBD-GSIM (red), MLP-GSIM (m=256, blue), and FSE (green) for test dataset.

of MBD-GSIM is conducted by using the graph type KTH indoor floorplan dataset as the training set and the test set, respectively, at rates of 90% and 10%. The data pairs are generated based on the random walk method (Figure 5).

For the analysis of MBD-GSIM based exploration planner, we compare the MBD-GSIM based planner with baseline exploration methods (FSE-GSIM based planner [5] and cost-based hector planner [8], [9]) in multiple indoor environments (the used environments are in Figure 11, 12, and 13). In the comparisons, we investigate whether the proposed method is effective to guide the robot to a space with a high probability of target presence. For that, various metrics such as representative snapshots during TDE scenarios, the graph of exploration speed for the space of high target existence probability, and the score of information gathering quality are provided. The score of the information gathering quality is defined as in Equation 23:

$$score = \int \gamma^{1+x} \left[\sum_{c_j \in \mathcal{C}} p(E_{c_j}^{o_t}) \Delta A_{c_j}(x) \right] dx \quad (23)$$

where $\Delta A_{c_j}(x)$ is the newly observed space with category c_j at traveled distance x and γ is the discounting factor.

C. RESULT

1) MBD-GSIM

Figure 9 shows the loss histories over episodes of MBD-GSIM and MLP-GSIM. The upper graphs of Figure 9 represent the loss histories of MLP-GSIM according to the network size m. Although the loss value drops significantly for the training set as m increases, For the test sets, loss tends to increase significantly after certain episodes. This is the typical trend of overfitting, which means that MLP-GSIM is not properly identifying the latent patterns from the semantic-spatial relation dataset of the indoor space. On the other hand, in the MBD-GSIM, the loss value drops with episodes almost equally in the training and test set. This means that the MBD-GSIM properly learns the latent context without overfitting. In addition, the final loss value is reduced as the limit length of BFS L becomes larger. The larger an area around the node of interest is referenced (as the L becomes larger), the better the performance. The tendency of the loss reduction remains the same in the space prediction accuracy (Figure 10). The ratio of space prediction accuracy between MLP-GSIM, FSE and MBD-GSIM is shown in Table 2. At $L = 1$, the mean accuracies of both methods are similar, but as L grows, MBD-GSIM performance becomes superior.

2) MBD-GSIM BASED FRONTIER EXPLORATION

Figure 11 and 12 represent representative snapshots during TDE scenarios in different indoor environments. Figure 11 is the scenarios in which the existence probability of target object in the toilet (blue region) is high ($p(E_C^{o_t})$ = [office, corridor, share, maintenance, toilet] = [0.1, 0.1, 0.1, 0.1, 0.6]). Based on the observed map (left), the abstracted graph representation is obtained (middle). The future space category $p(H_v^C)$ is predicted by MBD-GSIM
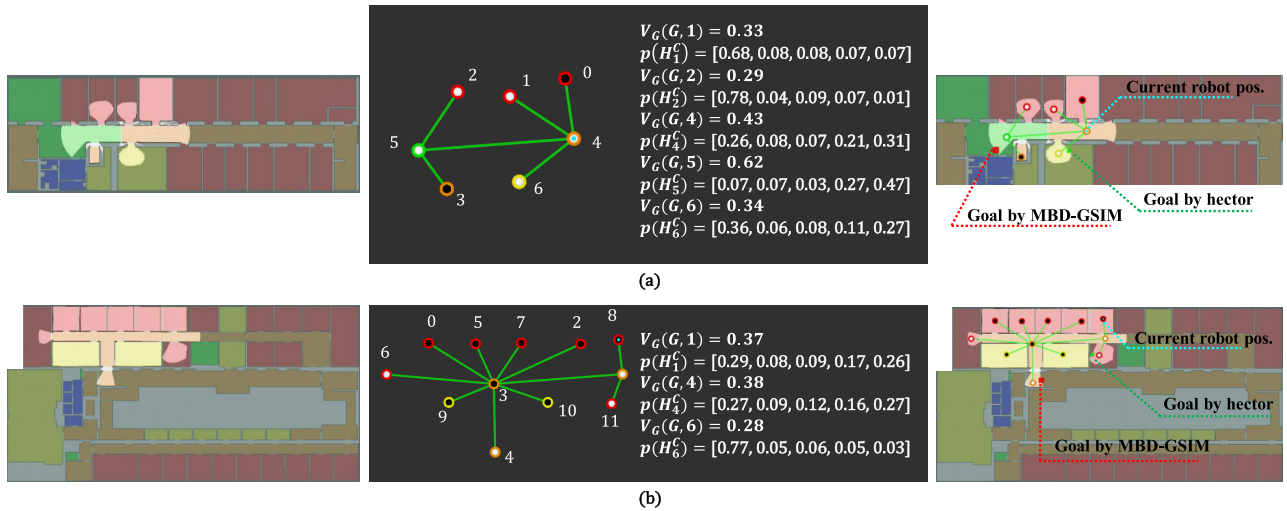
FIGURE 11. Representative snap shot of MBD-GSIM based frontier exploration when parameters are set to $p(E_C^{o_t}) = [0.1, 0.1, 0.1, 0.1, 0.6]$, $R = 3$, and $L = 3$. Left figure represents the ground truth map (dark background) and observed map (bright region). Middle figure is a graph of the observed map with estimated V_G and $p(H_v^{c_j})$. (shapes of nodes contain information about category of space (outer circle, color by categories), whether any frontier is in a neighbor (middle circle, white if frontiers are in neighbor, or black), and robot position (inner circle, cyan if robot is at the node)). Right figure represents the current robot position and generated goal point of MBD-GSIM based planner (red square) compared to cost-based frontier exploration (green square, Hector exploration planner [8], [9]).
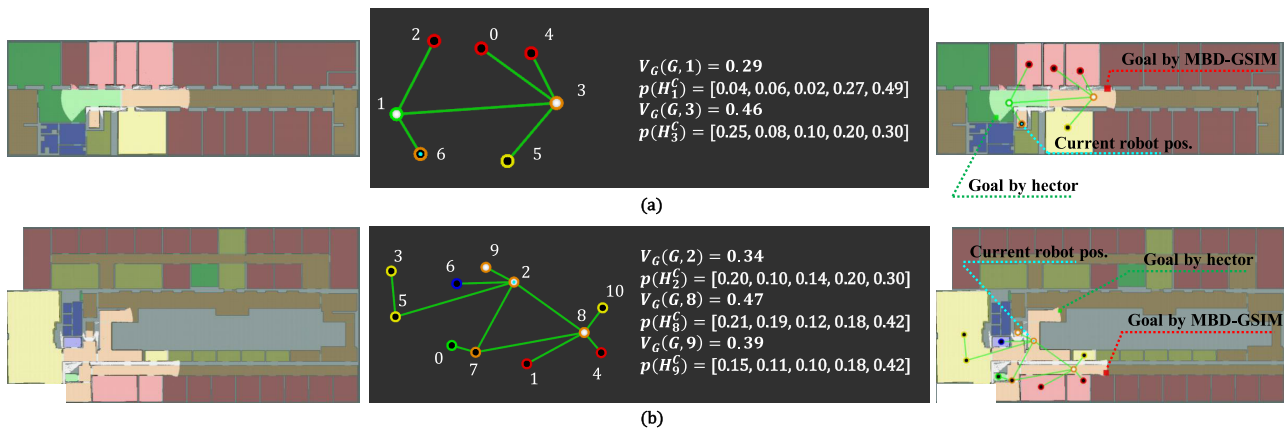

FIGURE 12. Representative snap shot of MBD-GSIM based frontier exploration when $p(E_C^{o_t}) = [0.6, 0.1, 0.1, 0.1, 0.1]$.

(with level $L = 4$), and the values of frontier nodes are estimated by rolling out up to length $R = 3$. The probability vector $p(H_v^C)$ in the figure is the one-step prediction of the space category. In the case of Figure 11-(a), Node 5 has the highest probability that the space over the node is the toilet, and the node value is also the highest, which is a desirable result. As a result, even though the robot is located around node 4 (the farthest from the toilet), the generated goal point is the frontier near node 5. On the contrary, the cost-based exploration method [8], [9] generates a goal nearest to the robot. Figure 11-(b) also shows the results in different environment. Figure 12 shows the scenarios when the target object is most likely to be in the office (red region, $p(E_C^{o_t}) = [0.6, 0.1, 0.1, 0.1, 0.1]$. In Figure 12, the robot is directed by the MBD-GSIM based planner to the right (node 3) in (a) and the lower right (node 8) in (b), where many offices are located.
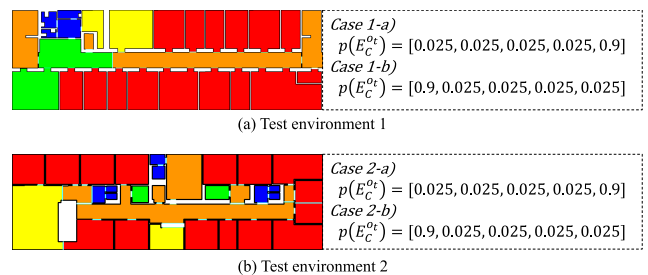

FIGURE 13. Experiment cases to measure the quality of information gathering. Each case differs according to the $p(E_C^{o_t})$ value and environment. Repetitive experiments are conducted by changing the initial position in each case.

The scores of information gathering quality (Equation 23) are also compared. Figures 13 shows the test cases according to different environments and target existence probability settings. In the two different maps, we calculate scores when the
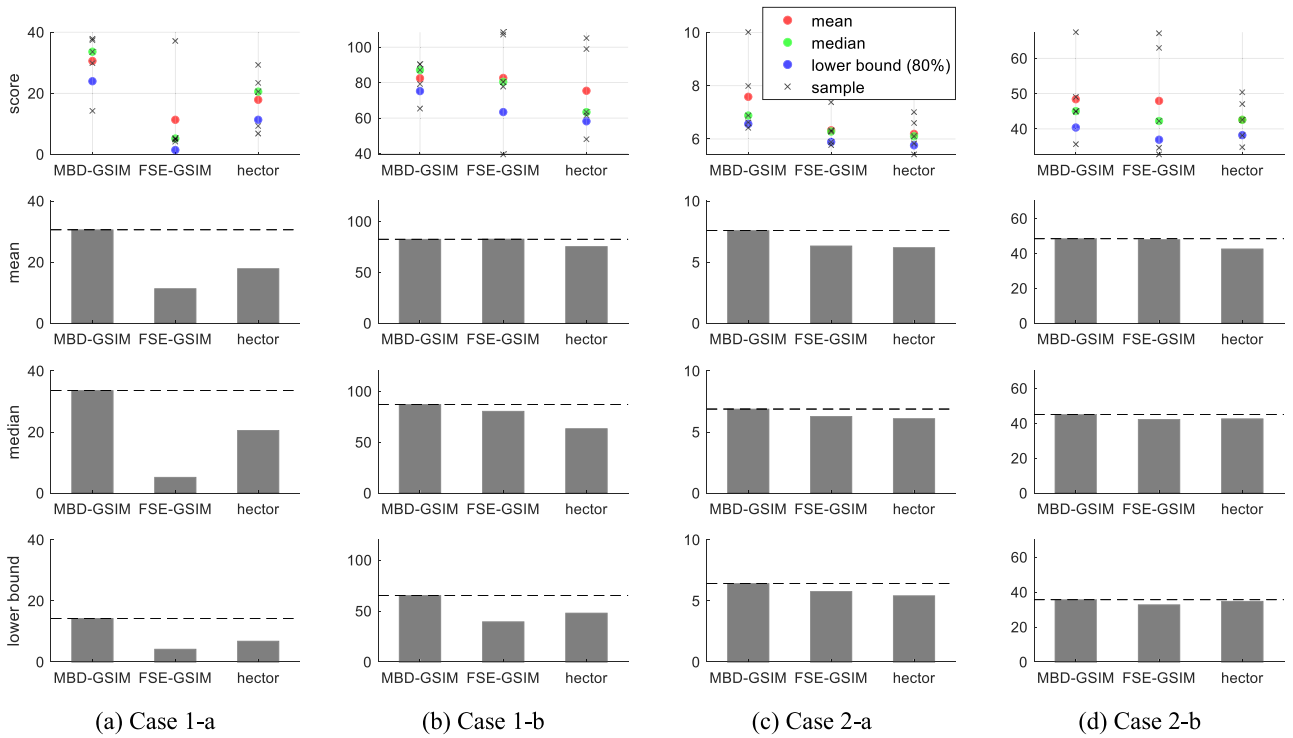
FIGURE 14. Information quality scores of MBD-GSIM based planner (ours), FSE-GSIM [5] and hector planner ([8], [9]).

TABLE 3. Information quality scores improvement ratio of MBD-GSIM based planner (ours) compared to FSE-GSIM [5] and hector planner [8], [9]. Mean, median and lower bound are investigated. Bold font means an improvement of more than 5 per cent. (M:MBD-GSIM-based planner, F:FSE-GSIM-based planner, h:hector planner.)

<div style="display:flex">

(a) Mean

case	1-a	1-b	2-a	2-b
M/F	**2.69**	1.00	**1.20**	1.01
M/h	**1.71**	**1.09**	**1.22**	**1.14**

(b) Median

case	1-a	1-b	2-a	2-b
M/F	**6.46**	**1.08**	**1.09**	**1.06**
M/h	**1.63**	**1.37**	**1.13**	**1.05**

(c) Lower bound (80% confidence)

case	1-a	1-b	2-a	2-b
M/F	**16.61**	**1.19**	**1.11**	**1.09**
M/h	**2.11**	**1.29**	**1.14**	**1.16**

</div>

TABLE 4. Kruskal-Wallis (KW) and Mann-Whitney (MW) tests for each experiment case. KW test is used for hypothesis testing of the three groups of samples (MBD-GSIM planner, FSE-GSIM planner, and hector planner). MW test is used for hypothesis testing of two groups. The hypothesis is: The samples come from the same distribution. If the hypothesis is rejected (✗, p-value< 0.1), it means that there is a meaningful difference between the methods. (M:MBD-GSIM-based planner, F:FSE-GSIM-based planner, h:hector planner.)

(a) KW test

	case 1-a	case 1-b	case 2-a	case 2-b
p-value	0.056	0.134	0.087	0.647
hypothesis	✗	✓	✗	✓

<div style="display:flex">

(b) MW test for case 1-a

	M↔F	M↔h	F↔h
p-value	0.047	0.047	0.117
hypothesis	✗	✗	✓

(c) MW test for case 1-b

	M↔F	M↔h	F↔h
p-value	0.917	0.601	0.465
hypothesis	✓	✓	✓

</div>

<div style="display:flex">

(d) MW test for case 2-a

	M↔F	M↔h	F↔h
p-value	0.047	0.075	0.754
hypothesis	✗	✗	✓

(e) MW test for case 2-b

	M↔F	M↔h	F↔h
p-value	0.465	0.465	0.917
hypothesis	✓	✓	✓

</div>

target existence probability is high in the toilet (blue region, $p(E_C^{o_t}) = [0.025, 0.025, 0.025, 0.025, 0.9]$) and office (red region, $p(E_C^{o_t}) = [0.9, 0.025, 0.025, 0.025, 0.025]$). For each

case, 5 iterations of the experiments are conducted changing the initial robot positions. Figure 14 and Table 3 represent the results. In the case of high probability in the toilet, the
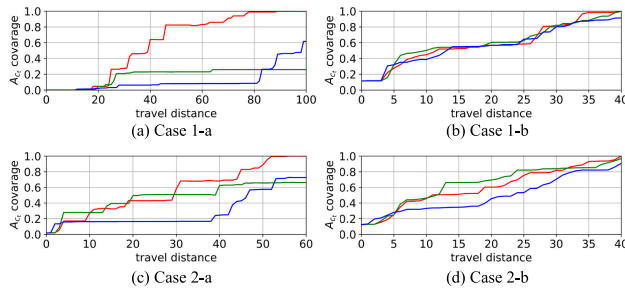
FIGURE 15. The average exploration speed for the space with the category of the highest target existence probability.

MBD-GSIM based planner is superior to the FSE-GSIM [5] and cost based planner (hector [8], [9]) in terms of mean, median, and lower bound of 80% confidence (case 1-a and 2-a in Figure 14 and Table 3). When the probability is high in the office (case 1-b and 2-b), the MBD-GSIM based planner is slightly better than the others but it is not more significant than the toilet case. It is because the impact of spatial inference is relatively low because offices are spaces that frequently appear in the entire region. This trend is supported in the statistical analysis in Table 4. According to the Kruskal-Wallis (KW) and Mann-Whitney (MW) tests, the MBD-GSIM based planner have outstanding performance difference (i.e., improvement) compared to the others in the case 1-a and 2-a. On the other hand, in case of the target existence probability is high in the office, the statistical tests represent the minor differences. These trends are also repeated in the exploration speed for the area with the category of the highest target existence probability (Table 15).

VIII. CONCLUSION AND FUTURE WORK

In this paper, an indoor target-directed exploration problem leveraging the semantic-spatial relation of a floorplan dataset was investigated. The suggested multivariate Bernoulli distribution based graphical space inference model (MBD-GSIM) and the space inference aided target-directed exploration planner was applied in the indoor environment of real buildings, and it shows that pattern cognitive model based space inferencing can be a feasible way to achieve efficient target search in indoor environments.

In the future, from a practical point of view, the frontier value estimation method can be strengthened by fusing various contexts related to the target (i.e., prior target position information, landmark (e.g., room number) based hints, and so on). In the theoretical point of view, the MBD-GSIM model can be developed in the direction of relaxing assumptions 3, 4, and 5. In this paper, using the assumptions, the MBD concept was successfully applied to the space inference, and high inference accuracy was obtained compared to the existing method. However, since information related to the interaction between spaces may be lost in the process of applying the assumptions, relaxing them can be a future work for better performance.

REFERENCES

[1] D. Joho, M. Senk, and W. Burgard, "Learning search heuristics for finding objects in structured environments," *Robot. Auto. Syst.*, vol. 59, no. 5, pp. 319–328, May 2011.

[2] T. Kollar and N. Roy, "Utilizing object-object and object-scene context when planning to find things," in *Proc. IEEE Int. Conf. Robot. Autom.*, May 2009, pp. 2168–2173.

[3] P. Viswanathan, D. Meger, T. Southey, J. J. Little, and A. K. Mackworth, "Automated spatial-semantic modeling with applications to place labeling and informed search," in *Proc. Can. Conf. Comput. Robot Vis.*, May 2009, pp. 284–291.

[4] L. Kunze, M. Beetz, M. Saito, H. Azuma, K. Okada, and M. Inaba, "Searching objects in large-scale indoor environments: A decision-theoretic approach," in *Proc. IEEE Int. Conf. Robot. Autom.*, May 2012, pp. 4385–4390.

[5] A. Aydemir, P. Jensfelt, and J. Folkesson, "What can we learn from 38,000 rooms? Reasoning about unexplored space in indoor environments," in *Proc. IEEE/RSJ Int. Conf. Intell. Robots Syst.*, Oct. 2012, pp. 4675–4682.

[6] A. Aydemir, A. Pronobis, M. Göbelbecker, and P. Jensfelt, "Active visual object search in unknown environments using uncertain semantics," *IEEE Trans. Robot.*, vol. 29, no. 4, pp. 986–1002, Aug. 2013.

[7] C. Wang, J. Cheng, J. Wang, X. Li, and M. Q.-H. Meng, "Efficient object search with belief road map using mobile robot," *IEEE Robot. Autom. Lett.*, vol. 3, no. 4, pp. 3081–3088, Oct. 2018.

[8] S. Wirth and J. Pellenz, "Exploration transform: A stable exploring algorithm for robots in rescue environments," in *Proc. IEEE Int. Workshop Saf., Secur. Rescue Robot.*, Sep. 2007, pp. 1–5.

[9] S. Kohlbrecher, J. Meyer, T. Graber, K. Petersen, U. Klingauf, and O. von Stryk, "Hector open source modules for autonomous mapping and navigation with rescue robots," in *Robot Soccer World Cup*. Berlin, Germany: Springer, 2013, pp. 624–631.

[10] B. Yamauchi, "A frontier-based approach for autonomous exploration," in *Proc. IEEE Int. Symp. Comput. Intell. Robot. Autom. CIRA Towards New Comput. Princ. Robot. Autom.*, Jul. 1997, pp. 146–151.

[11] B. Yamauchi, "Frontier-based exploration using multiple robots," in *Proc. 2nd Int. Conf. Auto. Agents (AGENTS)*, 1998, pp. 47–53.

[12] H. Umari and S. Mukhopadhyay, "Autonomous robotic exploration based on multiple rapidly-exploring randomized trees," in *Proc. IEEE/RSJ Int. Conf. Intell. Robots Syst. (IROS)*, Sep. 2017, pp. 1396–1402.

[13] A. Kamalova, K. D. Kim, and S. G. Lee, "Waypoint mobile robot exploration based on biologically inspired algorithms," *IEEE Access*, vol. 8, pp. 190342–190355, 2020.

[14] A. Andreopoulos, S. Hasler, H. Wersing, H. Janssen, J. K. Tsotsos, and E. Korner, "Active 3D object localization using a humanoid robot," *IEEE Trans. Robot.*, vol. 27, no. 1, pp. 47–64, Feb. 2011.

[15] S. Radmard and E. A. Croft, "Active target search for high dimensional robotic systems," *Auton. Robots*, vol. 41, no. 1, pp. 163–180, 2017.

[16] P.-E. Forssen, D. Meger, K. Lai, S. Helmer, J. J. Little, and D. G. Lowe, "Informed visual search: Combining attention and object recognition," in *Proc. IEEE Int. Conf. Robot. Autom.*, May 2008, pp. 935–942.

[17] Y. Xiao, S. Katt, A. T. Pas, S. Chen, and C. Amato, "Online planning for target object search in clutter under partial observability," in *Proc. Int. Conf. Robot. Autom. (ICRA)*, May 2019, pp. 8241–8247.

[18] C. Wang, J. Cheng, W. Chi, T. Yan, and M. Q.-H. Meng, "Semantic-aware informative path planning for efficient object search using mobile robot," *IEEE Trans. Syst., Man, Cybern. Syst.*, vol. 51, no. 8, pp. 5230–5243, Aug. 2021.

[19] S. Oßwald, M. Bennewitz, W. Burgard, and C. Stachniss, "Speeding-up robot exploration by exploiting background information," *IEEE Robot. Autom. Lett.*, vol. 1, no. 2, pp. 716–723, Jul. 2016.

[20] S. Bai, J. Wang, F. Chen, and B. Englot, "Information-theoretic exploration with Bayesian optimization," in *Proc. IEEE/RSJ Int. Conf. Intell. Robots Syst. (IROS)*, Oct. 2016, pp. 1816–1822.

[21] R. Shrestha, F.-P. Tian, W. Feng, P. Tan, and R. Vaughan, "Learned map prediction for enhanced mobile robot exploration," in *Proc. Int. Conf. Robot. Autom. (ICRA)*, May 2019, pp. 1197–1204.

[22] F. Niroui, K. Zhang, Z. Kashino, and G. Nejat, "Deep reinforcement learning robot for search and rescue applications: Exploration in unknown cluttered environments," *IEEE Robot. Autom. Lett.*, vol. 4, no. 2, pp. 610–617, Apr. 2019.

[23] L. Ly and Y.-H.-R. Tsai, "Autonomous exploration, reconstruction, and surveillance of 3D environments aided by deep learning," in *Proc. Int. Conf. Robot. Autom. (ICRA)*, May 2019, pp. 5467–5473.

[24] M. Saroya, G. Best, and G. A. Hollinger, "Online exploration of tunnel networks leveraging topological CNN-based world predictions," in *Proc. IEEE/RSJ Int. Conf. Intell. Robots Syst. (IROS)*, Oct. 2020, pp. 6038–6045.

[25] A. Aydemir, M. Göbelbecker, A. Pronobis, K. Sjöö, and P. Jensfelt, "Plan-based object search and exploration using semantic spatial knowledge in the real world," in *Proc. ECMR*, 2011, pp. 13–18.

[26] C. Jung and D. H. Shim, "Incorporating multi-context into the traversability map for urban autonomous driving using deep inverse reinforcement learning," *IEEE Robot. Autom. Lett.*, vol. 6, no. 2, pp. 1662–1669, Apr. 2021.

[27] J. Li, J. Wang, H. Peng, Y. Hu, and H. Su, "Fuzzy-torque approximation-enhanced sliding mode control for lateral stability of mobile robot," *IEEE Trans. Syst., Man, Cybern. Syst.*, early access, Jan. 28, 2021, doi: 10.1109/TSMC.2021.3050616.

[28] J. Li, H. Qin, J. Wang, and J. Li, "OpenStreetMap-based autonomous navigation for the four wheel-legged robot via 3D-LiDAR and CCD camera," *IEEE Trans. Ind. Electron.*, vol. 69, no. 3, pp. 2708–2717, Mar. 2022.

[29] R. F. Salas-Moreno, R. A. Newcombe, H. Strasdat, P. H. J. Kelly, and A. J. Davison, "SLAM++: Simultaneous localisation and mapping at the level of objects," in *Proc. IEEE Conf. Comput. Vis. Pattern Recognit.*, Jun. 2013, pp. 1352–1359.

[30] S. Sengupta, E. Greveson, A. Shahrokni, and P. H. S. Torr, "Urban 3D semantic modelling using stereo vision," in *Proc. IEEE Int. Conf. Robot. Autom.*, May 2013, pp. 580–585.

[31] Z. Zhao and X. Chen, "Building 3D semantic maps for mobile robots using RGB-D camera," *Intell. Service Robot.*, vol. 9, no. 4, pp. 297–309, Oct. 2016.

[32] X. Li, H. Ao, R. Belaroussi, and D. Gruyer, "Fast semi-dense 3D semantic mapping with monocular visual SLAM," in *Proc. IEEE 20th Int. Conf. Intell. Transp. Syst. (ITSC)*, Oct. 2017, pp. 385–390.

[33] M. Yan, J. Wang, J. Li, K. Zhang, and Z. Yang, "Traffic scene semantic segmentation using self-attention mechanism and bi-directional GRU to correlate context," *Neurocomputing*, vol. 386, pp. 293–304, Apr. 2020.

[34] K. Tateno, F. Tombari, I. Laina, and N. Navab, "CNN-SLAM: Real-time dense monocular SLAM with learned depth prediction," in *Proc. IEEE Conf. Comput. Vis. Pattern Recognit. (CVPR)*, Jul. 2017, pp. 6243–6252.

[35] J. Li, X. Zhang, J. Li, Y. Liu, and J. Wang, "Building and optimization of 3D semantic map based on LiDAR and camera fusion," *Neurocomputing*, vol. 409, pp. 394–407, Oct. 2020.

[36] X. Tu, J. Zhang, R. Luo, K. Wang, Q. Zeng, Y. Zhou, Y. Yu, and S. Du, "Reconstruction of high-precision semantic map," *Sensors*, vol. 20, no. 21, p. 6264, Nov. 2020.

[37] M. Haklay and P. Weber, "OpenStreetMap: User-generated street maps," *IEEE Pervasive Comput.*, vol. 7, no. 4, pp. 12–18, Oct. 2008.

[38] B. Suger and W. Burgard, "Global outer-urban navigation with OpenStreetMap," in *Proc. IEEE Int. Conf. Robot. Autom. (ICRA)*, May 2017, pp. 1417–1422.

[39] F. Boniardi, T. Caselitz, R. Kummerle, and W. Burgard, "Robust LiDAR-based localization in architectural floor plans," in *Proc. IEEE/RSJ Int. Conf. Intell. Robots Syst. (IROS)*, Sep. 2017, pp. 3318–3324.

[40] S. L. Bowman, N. Atanasov, K. Daniilidis, and G. J. Pappas, "Probabilistic data association for semantic SLAM," in *Proc. IEEE Int. Conf. Robot. Autom. (ICRA)*, May 2017, pp. 1722–1729.

[41] A. Rosinol, M. Abate, Y. Chang, and L. Carlone, "Kimera: An open-source library for real-time metric-semantic localization and mapping," in *Proc. IEEE Int. Conf. Robot. Autom. (ICRA)*, May 2020, pp. 1689–1696.

[42] A. Rosinol, A. Violette, M. Abate, N. Hughes, Y. Chang, J. Shi, A. Gupta, and L. Carlone, "Kimera: From SLAM to spatial perception with 3D dynamic scene graphs," 2021, *arXiv:2101.06894*.

[43] H. M. Choset, K. M. Lynch, S. Hutchinson, G. Kantor, W. Burgard, L. Kavraki, S. Thrun, and R. C. Arkin, *Principles of Robot Motion: Theory, Algorithms, and Implementation*. Cambridge, MA, USA: MIT Press, 2005.

[44] A. Kneidl, A. Borrmann, and D. Hartmann, "Generation and use of sparse navigation graphs for microscopic pedestrian simulation models," *Adv. Eng. Informat.*, vol. 26, no. 4, pp. 669–680, Oct. 2012.

[45] Y. Pang, L. Zhou, B. Lin, G. Lv, and C. Zhang, "Generation of navigation networks for corridor spaces based on indoor visibility map," *Int. J. Geograph. Inf. Sci.*, vol. 34, no. 1, pp. 177–201, Jan. 2020.

[46] H. Oleynikova, Z. Taylor, R. Siegwart, and J. Nieto, "Sparse 3D topological graphs for micro-aerial vehicle planning," in *Proc. IEEE/RSJ Int. Conf. Intell. Robots Syst. (IROS)*, Oct. 2018, pp. 1–9.

[47] Q. Wang, M. Langerwisch, and B. Wagner, "Wide range global path planning for a large number of networked mobile robots based on generalized Voronoi diagrams," *IFAC Proc. Volumes*, vol. 46, no. 29, pp. 107–112, 2013.

[48] B. Binder, F. Beck, F. Konig, and M. Bader, "Multi robot route planning (MRRP): Extended spatial-temporal prioritized planning," in *Proc. IEEE/RSJ Int. Conf. Intell. Robots Syst. (IROS)*, Nov. 2019, pp. 4133–4139.

[49] J. A. Nelder and R. W. Wedderburn, "Generalized linear models," *J. Roy. Stat. Soc., Gen.*, vol. 135, no. 3, pp. 370–384, 1972.

[50] F. Gao, G. Wahba, R. Klein, and B. Klein, "Smoothing spline ANOVA for multivariate Bernoulli observations with application to ophthalmology data," *J. Amer. Stat. Assoc.*, vol. 96, no. 453, pp. 127–160, Mar. 2001.

[51] S. Ding, G. Wahba, and J. X. Zhu, "Learning higher-order graph structure with features by structure penalty," in *Proc. Neural Inf. Process. Syst.*, Princeton, NJ, USA: Citeseer, 2011, pp. 253–261.

[52] B. Dai, S. Ding, and G. Wahba, "Multivariate Bernoulli distribution," *Bernoulli*, vol. 19, no. 4, pp. 1465–1483, 2013.

[53] C. Tran, W.-Y. Shin, A. Spitz, and M. Gertz, "DeepNC: Deep generative network completion," *IEEE Trans. Pattern Anal. Mach. Intell.*, early access, Oct. 19, 2020, doi: 10.1109/TPAMI.2020.3032286.

[54] X. Wang and J. Yin, "Relaxed multivariate Bernoulli distribution and its applications to deep generative models," in *Proc. Conf. Uncertainty Artif. Intell.*, 2020, pp. 500–509.

[55] A. Narayanan, M. Chandramohan, R. Venkatesan, L. Chen, Y. Liu, and S. Jaiswal, "Graph2vec: Learning distributed representations of graphs," 2017, *arXiv:1707.05005*.

WOO-CHEOL LEE (Student Member, IEEE) received the B.S. degree in aerospace engineering from Korea Aerospace University, Goyang, South Korea, in 2015, and the M.S. degree in aerospace engineering from the Korea Advanced Institute of Science and Technology (KAIST), Daejeon, South Korea, in 2017, where he is currently pursuing the Ph.D. degree in aerospace engineering. His current research interests include estimation and control in uncertain environment.
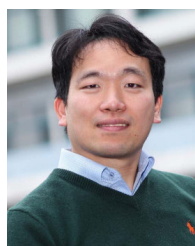
HAN-LIM CHOI (Senior Member, IEEE) received the B.S. and M.S. degrees in aerospace engineering from the Korea Advanced Institute of Science and Technology (KAIST), Daejeon, South Korea, in 2000 and 2002, respectively, and the Ph.D. degree in aeronautics and astronautics from the Massachusetts Institute of Technology (MIT), Cambridge, MA, USA, in 2009. Then, he studied at MIT as a Postdoctoral Associate until he joined KAIST, in 2010. He is currently a Professor of aerospace engineering at KAIST. His current research interests include estimation and control for sensor networks and decision making for multi-agent systems. He was a recipient of the Automatic Applications Prize, in 2011 (together with Dr. Jonathan P. How).

● ● ●